

# Generalized phase diversity for wave-front sensing

Heather I. Campbell, Sijiong Zhang, and Alan H. Greenaway

*School of Engineering and Physical Sciences, Heriot-Watt University, Riccarton, Edinburgh EH14 4AS, Scotland, UK*

Sergio Restaino

*Naval Research Laboratory, Remote Sensing Division, Code 721, Kirtland Air Force Base, Albuquerque, New Mexico*

Received July 15, 2004

Phase diversity is a phase-retrieval algorithm that uses a pair of intensity images taken symmetrically about the wave front to be determined. If these images are taken about the system input pupil this is equivalent to a curvature-sensing algorithm. Traditionally a defocus aberration kernel is used to produce the phase-diverse data. We present a generalization of this method to allow the use of other functions as the diversity kernel. We discuss the necessary and sufficient conditions that such a function must satisfy for use in a null wave-front sensor. Computer simulations were used to validate these results. © 2004 Optical Society of America  
*OCIS codes:* 010.0010, 010.1080, 010.7350.

Phase diversity (PD) can be used as an algorithm for the reconstruction of wave-front phase from intensity images captured in two planes symmetrically placed about the wave front to be determined and normal to the axis of propagation.<sup>1-3</sup> When these measurement planes are symmetric about the pupil of the system, PD becomes a curvature-sensing system.<sup>4</sup> Figure 1 is a schematic of the measurement and wave-front (pupil) planes that shows how the curvature of a distorted wave front affects the intensity in the measurement planes. Portions of the wave front that are locally concave will propagate toward a focus and produce a higher-intensity spot on the second measurement plane than was seen on the first. The opposite is true for convex portions of the wave front, which diverge as they propagate. The intensity difference between the measurement planes is indicative of the location, direction, and magnitude of the wave-front curvature.

It has been shown that a quadratically distorted diffraction grating can be used to simultaneously image multiple object planes onto a single detector.<sup>5</sup> The diffraction grating provides a different level of defocus in each diffraction order and the intensity images formed on a CCD detector provide data for the PD algorithm. The wave front is then reconstructed using a Green's function solution to the differential intensity transport equation.<sup>6</sup> The defocus phase diversity (DPD) wave-front sensor can provide real-time data reduction with high (subnanometer) accuracy.<sup>7</sup>

Assumptions imposed by use of the Green's function involve the uniformity of the input intensity within the pupil, the continuity of the wave-front phase, and the continuity of the first derivative (the slope) of the phase.<sup>6</sup> These assumptions limit the DPD wave-front sensor's performance with scintillated or discontinuous wave fronts and also potentially exclude the use of pixelated corrective elements; one of the most cost effective, versatile, and lightweight modulator solutions for adaptive optics systems.<sup>8</sup> In this Letter we will consider how to overcome these limitations through generalization of the PD method.

The generalized phase diversity (GPD) method, like the DPD sensor, will use two intensity images

to perform wave-front sensing. However, DPD's use of two images that are symmetrically defocused with respect to the unknown wave front is replaced in GPD by a pair of images of the wave-front plane, each convolved with arbitrary but related aberration functions. These functions may include, but will not be limited to, defocus. By analyzing the GPD sensor as a simple null sensor we restrict the permitted aberration functions to those with certain symmetries.

A sufficient condition for operation of the null sensor is that it provides a null output for a plane, undistorted input wave front and will generate an error signal when aberrations are present. This signal should ideally encode the position, direction, and amplitude of the wave-front error. Let us consider the input wave front at the pupil plane to be

$$\Psi(r) = |\Psi(r)|\exp[i\varphi(r)], \quad (1)$$

where  $r$  is the coordinate in the pupil plane. The Fourier transform of Eq. (1) can be expressed as

$$\psi(\xi) = H(\xi) + A(\xi), \quad (2)$$

where  $H(\xi)$  is the Hermitian component [the transform of the purely real part of  $\Psi(r)$ ] and  $A(\xi)$  is the anti-Hermitian component (the transform of the purely

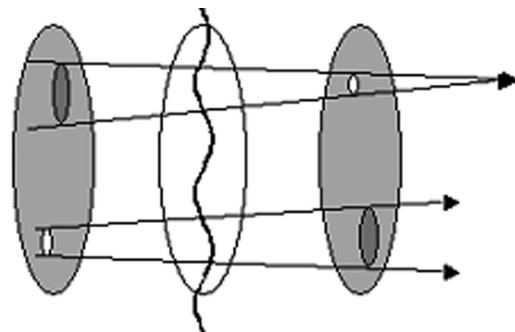


Fig. 1. Schematic of the measurement and wave-front planes showing the connection between wave-front shape and intensity.

imaginary part). The symmetries of these components will be required later and can be expressed as

$$H(\xi) = H^*(-\xi), \quad A(\xi) = -A^*(-\xi). \quad (3)$$

The aberration kernel that we choose to apply for GPD will be encoded into a diffraction grating as a complex filter function  $F_{\pm}(\xi)$ , whose Fourier transform  $f_{\pm}(r)$  is convolved with  $\Psi(r)$ . The filter function has the form  $F_{\pm}(\xi) = R(\xi) \pm iI(\xi)$ , where  $R(\xi)$  is the real part and  $I(\xi)$  is the imaginary part of  $F_{\pm}(\xi)$ . We are particularly interested in the symmetries of  $R(\xi)$  and  $I(\xi)$ , which will provide us with a useful null sensor. These allowed symmetries will form the basis of the necessary conditions for the GPD wave-front sensor.

If  $j_+(r)$  is the intensity image in the +1 diffraction order and  $j_-(r)$  is the intensity in the -1 diffraction order, the detected intensity functions can be expressed algebraically as

$$j_{\pm}(r) = \left| \int d\xi \psi(\xi) F_{\pm}(\xi) \exp(-i\xi r) \right|^2. \quad (4)$$

We are interested in the difference in intensity between these two images:

$$\begin{aligned} d(r) &= j_+(r) - j_-(r) \\ &= 2i \left[ \int d\xi \psi(\xi) I(\xi) \exp(-ir\xi) \right. \\ &\quad \times \int d\xi' \psi^*(\xi') R(\xi') \exp(ir\xi') \\ &\quad - \int d\xi \psi(\xi) R(\xi) \exp(-ir\xi) \\ &\quad \left. \times \int d\xi' \psi^*(\xi') I(\xi') \exp(ir\xi') \right]. \quad (5) \end{aligned}$$

Note that  $d(r)$  in Eq. (5) is a real-valued function, since the quantity in brackets is a difference between two complex conjugates and is thus purely imaginary. Substituting from Eq. (2) into Eq. (5) and expanding and grouping terms gives

$$\begin{aligned} &\int d\xi H(\xi) I(\xi) \exp(-ir\xi) \int d\xi' H^*(\xi') R(\xi') \exp(ir\xi') \\ &- \int d\xi H(\xi) R(\xi) \exp(-ir\xi) \int d\xi' H^*(\xi') I(\xi') \exp(ir\xi'), \quad (6.1) \end{aligned}$$

$$\begin{aligned} &\int d\xi H(\xi) I(\xi) \exp(-ir\xi) \int d\xi' A^*(\xi') R(\xi') \exp(ir\xi') \\ &- \int d\xi A(\xi) R(\xi) \exp(-ir\xi) \int d\xi' H^*(\xi') I(\xi') \exp(ir\xi'), \quad (6.2) \end{aligned}$$

$$\begin{aligned} &\int d\xi A(\xi) I(\xi) \exp(-ir\xi) \int d\xi' H^*(\xi') R(\xi') \exp(ir\xi') \\ &- \int d\xi H(\xi) R(\xi) \exp(-ir\xi) \int d\xi' A^*(\xi') I(\xi') \exp(ir\xi'), \quad (6.3) \end{aligned}$$

$$\begin{aligned} &\int d\xi A(\xi) I(\xi) \exp(-ir\xi) \int d\xi' A^*(\xi') R(\xi') \exp(ir\xi') \\ &- \int d\xi A(\xi) R(\xi) \exp(-ir\xi) \int d\xi' A^*(\xi') I(\xi') \exp(ir\xi'); \quad (6.4) \end{aligned}$$

$d(r)/2i$  is the sum of expressions (6.1)–(6.4). These expressions are generally valid, and no limiting assumptions have so far been placed on the wave front. All the terms contain either  $R(\xi)$  or  $I(\xi)$ , so we immediately see that any filter function used in a GPD wave-front sensor must be complex. If either  $R(\xi)$  or  $I(\xi)$  is zero  $\forall \xi$ ,  $d(r)$  will provide a null output for all input wave fronts. In each expression [(6.1)–(6.4)] the two pairs of integrals are term by term the complex conjugates of each other. We also note that (6.1) and (6.4) contain only Hermitian or anti-Hermitian terms. Expressions (6.2) and (6.3) contain cross terms, where each integral pair contains a Hermitian and an anti-Hermitian component. Now let us consider the different symmetries of the real and imaginary parts that we could use to build the filter function.

First let us consider  $d(r)$  when the real and imaginary parts are both even functions of  $\xi$ . In expression (6.1) we see that each integral is purely real valued because of the symmetry of  $H(\xi)$  [see Eq. (3)] and the fact that  $I(\xi)$  and  $R(\xi)$  are both real valued and symmetric. Since each term in (6.1) is real-valued  $\forall \psi$ , this difference of two complex conjugates will be 0  $\forall \psi$ . Similarly, expression (6.4) is also always zero. Our null sensor signal is therefore a combination of (6.2) and (6.3). A plane wave is defined as a wave front with constant phase. Without any loss of generality we can assume this phase to be zero, and therefore the plane wave front is a purely real function with a purely Hermitian transform. For a purely real input wave front [i.e.,  $A(\xi) = 0$ ] each of the integral pairs in expressions (6.2) and (6.3) reduces to zero and a null output is obtained. Any input wave front with nonzero real and imaginary parts, as is the case with a distorted wave front, will produce an error signal. Similarly, when the real and imaginary parts of  $F_{\pm}(\xi)$  are both odd functions of  $\xi$ , the integrands in expression (6.1) are all purely anti-Hermitian and the integrands in (6.4) are purely Hermitian, and both expressions will therefore be 0  $\forall \psi$ . Thus  $d(r)$  again reduces to the sum of expressions (6.2) and (6.3). Filter functions with suitable symmetries can be composed of Zernike polynomials that, when expressed in polar form, have the radius  $\rho$  raised to an even power and even multiples of the angle  $\theta$ .

Now let us consider mixed symmetries; i.e., one of  $R(\xi)$  and  $I(\xi)$  is odd and one is even. By the same

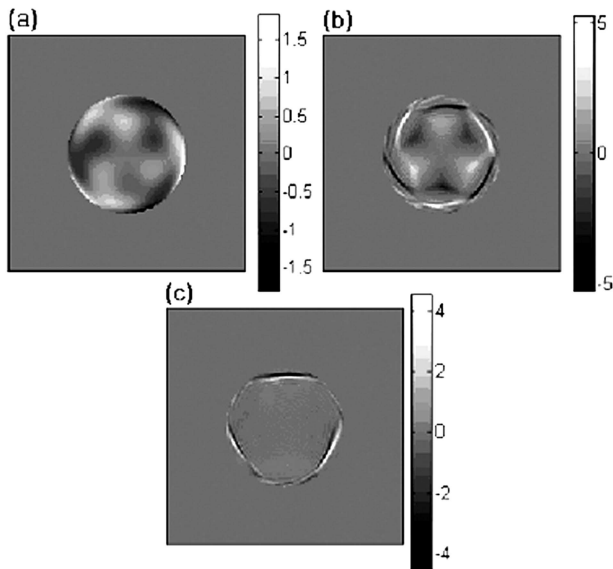


Fig. 2. Error signals  $d(r)$ , produced for (a) a distorted test wave front, using (b) a spherical aberration filter function and (c) a defocus filter function.

argument that reduced expressions (6.1) and (6.4) to zero in the previous case, this time (6.2) and (6.3) cancel. The error signal therefore becomes dependent on the sum of expressions (6.1) and (6.4). In (6.1) and (6.4) the mixture of odd and even symmetry leads to the result that one integral in each expression is purely real valued and the other is purely imaginary. It can be clearly shown that for a purely real plane-wave input an error signal will thus be generated by this filter function. For the sum of expressions (6.1) and (6.4) to generate a null output  $\forall r$  at least one integral in each pair must reduce to zero. This is not possible with anything other than trivial inputs. Such filter functions are therefore not suitable for use in a null sensor.

A GPD wave-front sensor that is based on a filter function with similar symmetry (complex even or complex odd) will have a difference function as in expressions (6.2) and (6.3) containing only cross terms. If the sign of the wave-front phase changes then, as a result of the symmetry of  $A(\xi)$ , the sign of the difference function  $d(r)$  will also change. Thus the difference signal will encode the sense of the error.

The location of the error on the wave front is directly related to  $a(r)$  [the transform of  $A(\xi)$ ]. If the filter function with which the input wave front is convolved has a maximum at the origin, then the position of the wave-front error will be localized about the point that  $a(r)$  is nonzero. For a GPD wave-front sensor designed to take the intensity images in the pupil plane there will be a direct 1–1 mapping between the position of the error on the wave front and its position on the intensity image.

Computer simulations were conducted to validate the analysis presented here and to explore the possibility of optimization of the filter function given *a priori*

information about the wave-front error. These simulations showed that significant error signals are generated for mixed symmetry filters with both plane and distorted input wave fronts. Similar symmetry filters were tested, and it was confirmed that these gave significant signal for distorted wave fronts, whereas for plane wave fronts the signal was in the zero to within rounding error.

Figure 2 shows simulated error signals  $d(r)$  for a distorted test wave front, with a spherical aberration filter function, and with a defocus filter function. As Figs. 2(b) and 2(c) demonstrate, a similar error signal amplitude is generated in both cases. These figures also show that the error signal profile produced by spherical aberration represents more faithfully the input pupil phase and shows a 1–1 mapping between the position of the wave-front error in the pupil and its position in the difference of the intensity images. In the defocus case the error signal shows the pupil phase, but with much lower contrast, as Fig. 2(c) shows.

It is not necessary, but it is sometimes desirable, to reconstruct the wave front. We ran further simulations, using an iterative Gerchberg–Saxton approach, to study wave-front reconstruction using different phase diversity kernels. A GPD wave-front sensing system can use pure Zernikes, combinations of Zernike functions, or other types of function that satisfy the symmetry conditions. In cases where *a priori* information about the wave-front errors is available, this information can be used to choose a diversity kernel appropriate to the application. Our simulations have shown that, unless it is known *a priori* that the test wave front is asymmetric, greater sensitivity is achieved when one is using symmetric filter functions. The potential to optimize GPD filter functions for particular applications and optimize sensitivity for detection of the most common errors present in a system will be explored in future publications.

This work was funded by the Particle Physics and Astronomy Research Council, the Defence Science and Technology Laboratory, and the European Office of Aerospace Research & Development. H. I. Campbell's e-mail address is H.I.Campbell@hw.ac.uk.

## References

1. R. A. Gonsalves, *Opt. Eng.* **21**, 829 (1982).
2. M. R. Teague, *J. Opt. Soc. Am.* **72**, 1199 (1982).
3. P. Schiske, *J. Phys. D Appl. Phys.* **8**, 1372 (1975).
4. F. Roddier, *Appl. Opt.* **27**, 1223 (1988).
5. P. M. Blanchard and A. H. Greenaway, *Appl. Opt.* **38**, 6692 (1999).
6. S. C. Woods and A. H. Greenaway, *J. Opt. Soc. Am. A* **20**, 508 (2003).
7. S. Djidel and A. H. Greenaway, in *3rd International Workshop on Adaptive Optics in Industry and Medicine* (Starline, Albuquerque, N.M., 2002), pp. 213–219.
8. D. C. Dayton, S. L. Browne, S. P. Sandven, J. D. Goglewski, and A. V. Kudryashov, *Appl. Opt.* **37**, 5579 (1998).